ISSN 0031-918X, Physics of Metals and Metallography, 2021, Vol. 122, No. 4, pp. 362–369. © Pleiades Publishing, Ltd., 2021.
Russian Text © The Author(s), 2021, published in Fizika Metallov i Metallovedenie, 2021, Vol. 122, No. 4, pp. 388–395.

STRUCTURE, PHASE TRANSFORMATIONS, AND DIFFUSION

Electron-Microscopy Investigation of Excess-Phase Precipitates Affecting the Intergranular Corrosion of Chromium–Nickel Austenitic Steels

A. N. Maznichevskii[a, b, *], Yu. N. Goikhenberg[b, **], and R. V. Sprikut[a, *]**

[a] *OOO Lasmet, Chelyabinsk, 454047 Russia*

[b] *South Ural State University, Chelyabinsk, 454080 Russia*

**e-mail: al.mazn@ya.ru*

***e-mail: goikhenbergyn@susu.ru*

****e-mail: mail@lasmet.ru*

Received July 24, 2020; revised September 3, 2020; accepted October 29, 2020

Abstract—Electron microscopic studies have been performed to investigate carbides, nitrides, and carbonitrides precipitated in chromium-nickel austenitic steels, which have been alloyed with nitrogen, silicon, boron, and rare-earth metals (REM) in different concentrations, and affecting the intergranular corrosion in these steels in highly-oxidizing environments. The intergranular corrosion has been found to result mainly from heating-induced precipitation of chromium carbides or carboborides, such as $Cr_{23}(C, B)_6$, which deplete the border areas of chromium to a greater extent than nitrides. The low corrosion rate corresponds to a lower dislocation number density. Concentrations of boron and REMs that do not have a negative effect on intergranular corrosion have been found.

Keywords: fine structure, intergranular corrosion, nitrogen, silicon, sensibilization, corrosion rate, microalloying, boron, rare earth metals, carbides, nitrides, borides

DOI: 10.1134/S0031918X2103011X

INTRODUCTION

The influence of alloying elements, such as silicon (of 0.2–1.0 wt % percentage, which is a component of many austenitic steels), nitrogen, boron, and rare earth metals (REMs) on the intergranular corrosion (IGC) of stainless steels in highly oxidizing environments remains a controversial issue [1–3].

The introduction of silicon into chromium-nickel stainless steels as an alloying element enhances their corrosion resistance [3–5]. However, an increased silicon content deteriorates the ductility of steels during hot forming [6]. Meanwhile, small additions of REMs and boron improve the formability of austenitic alloys during hot deformation [7, 8], but their effect on corrosion resistance is poorly understood.

It is noteworthy that, along with nitrogen-free stainless steels, there are also corrosion-resistant steels alloyed with nitrogen and silicon, which have high strength, ductility, resistance to corrosion cracking, wear resistance, and low friction coefficient [9–12].

The aim of this work is to carry out electron microscopic studies of the precipitation of excess phases affecting the corrosion resistance of chromium-nickel austenitic steels with different nitrogen and silicon concentrations and microalloyed with boron and rare-earth metals.

EXPERIMENTAL

Austenitic Cr–Ni (03Kh18N11) steels microalloyed with boron and rare earth metals and with a silicon concentration from 0.14 to 0.78 wt % and nitrogen concentration from 0.16 to 0.30 wt % were melted out (Table 1). The effect of boron and REMs on the corrosion resistance of steel was studied after fractional casting of melts. Boron or REMs were added to one of the ingots containing 0.38 wt % silicon or 0.30 wt % nitrogen. The ingots were deformed by smith forging and rolling to form billets of the required cross section under the conditions used for deformation of stainless austenitic steels. Stainless steels billets under study were subjected to austenitization in water from temperatures 1050 to 1150°C. Sensitization heating was carried out in the 500 to 850°C temperature range and a time range of 1 to 100 h.

The microstructure of the steels was examined using a Carl Zeiss Axio Observer optical microscope. To study the fine structure, thin foils were examined by transmission electron microscopy (TEM) using a

Table 1. Chemical composition of the investigated steels

Steel	Chemical composition, wt %						
	C	Si	Mn	Cr	Ni	N	*
3Kh18N11	0.024	0.65	0.95	18.34	11.07	0.05	–
2Kh18N11GS0.14	0.024	0.65	0.95	18.34	11.07	0.05	–
2Kh18N11GS0.38	0.022	0.14	1.02	17.82	11.21	0.05	–
2Kh18N11GS0.38R	0.021	0.38	1.00	17.80	11.20	0.04	–
2Kh18N11GS0.38Ch	0.021	0.38	1.00	17.80	11.20	0.04	0.0015 B
2Kh18N11GS0.78	0.021	0.38	1.00	17.80	11.20	0.04	0.042 Ce
3Kh18N11GS0.78	0.020	0.78	1.02	17.82	11.21	0.05	–
3Kh18N11G1A0.16	0.030	0.78	1.01	17.80	11.20	0.05	–
3Kh20N9G3A0.30	0.022	0.56	1.35	18.30	11.11	0.16	–
3Kh20N9G3A0.29R	0.025	0.30	3.02	20.26	9.60	0.30	–
3Kh20N9G3A0.29Ch	0.023	0.30	3.02	20.30	9.60	0.29	0.0015B; 0.0024B; 0.01B

All steels contain (less than or equal to) 0.015 S, 0.014 P, and 0.03 Ti wt %. Microalloying elements are indicated with "*".

Table 2. Corrosion resistance of the quenched stainless steels in a boiling 27% HNO_3 + 4 g/L Cr^{+6} solution

Concentration of an element		Average corrosion rate, mm/year	IGC penetration depth, mm
C, wt %	Si, wt %		
0.022	0.14	1.388	0.025
0.021	0.38	3.327	0.137
0.020	0.78	5.860	0.192

JEOL 2000EXI electron microscope at an accelerating voltage to 200 kV. Discs 3 mm in diameter and 1 mm thick were cut from samples after corrosion tests to prepare foils. Phase components were identified using electron diffraction patterns, bright-field, and dark-field images.

The samples for corrosion tests were prepared according to State Standard GOST 6032–2017 (and the tests were performed via technique whose Russian Specification DU corresponds to the "Advanced [Accelerated] Tests" carried out in boiling 65% nitric acid). The tests were conducted in a boiling 65% aqueous nitric acid solution for five cycles (48 h each). The tests under severe conditions were carried out in a solution with 27% HNO_3 and 4 g/L Cr^{+6} at boiling temperature. Cr^{+6} ions were introduced into the solution in the form of potassium dichromate $K_2Cr_2O_7$ addition. All tests were carried out under constant microscope observation of the thin sections.

The corrosion rate was determined by the weight loss of two samples which were tested simultaneously and independently of each other. A metallographic section was prepared on one of these samples to monitor the etching behavior of the steel using a microscope. A cross-sectional cut was made on one of these two samples after corrosion resistance testing. The cut was then ground and polished to measure the depth of intergranular corrosion penetration.

The corrosion rate of 0.5 mm/year was taken as the maximum allowable (critical) level of corrosion losses as required by GOST 6032–2017.

RESULTS AND DISCUSSION

Etching (intergranular corrosion) in the quenched nitrogen-free 03Kh18N11 (AISI 304L) steel with a low silicon content (0.14 wt %) occurred both along grain boundaries and, mainly, along twin boundaries. Grain boundaries were etched weakly and nonuniformly. The degree of etching of grain boundaries increases with increasing silicon content to 0.38 wt % and turned out to be comparable with the degree of etching of twin boundaries. At a silicon content of 0.78 wt %, grain boundaries begin to etch more actively than twin boundaries. The average corrosion rate of steels (0.20–0.25 mm/year) is more than twice lower than the maximum allowable level of corrosion losses and is independent of the silicon concentration.

Electron microscopic examination of grain boundaries in quenched steels (T_q = 1080, 1150°C) did not reveal any excessive phases at the grain boundaries, which indicates that the steels possess high corrosion resistance.

To estimate how the silicon concentration influences the resistance of the quenched samples to intergranular corrosion under oxidizing conditions, the tests were made more severe by introducing Cr^{+6} ions into the solution (Table 2). All the samples show high

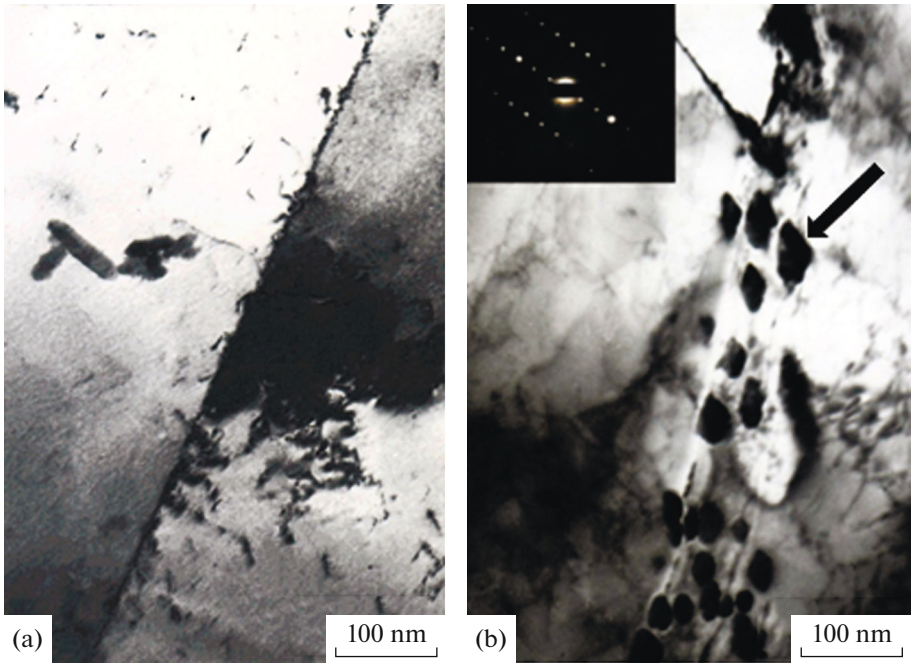

Fig. 1. TEM image of grain boundaries in (a) 02Kh18N11GS0.14 and (b) 02Kh18N11GS0.78 steels after quenching and sensitization heating at 650°C for 10 h. Figure 1b shows an electron diffraction pattern with a ⟨120⟩ zone axis, which was taken from the selected place indicated by the arrow.

tendency to IGC under severe test conditions with Cr^{+6} ions. However, the silicon concentration clearly affects the steel corrosion. Grain exfoliation from the surface of high-silicon 02Kh18N11GS0.78 steel samples was observed even during the first test cycle, while the same phenomenon from the surface of samples with lower silicon content (0.14, 0.38%) was observed only during the second test cycle.

The corrosion resistance of stainless steels after sensitization heating is more important to investigate (Table 3). The corrosion losses of the steel can be seen to increase with increasing silicon content. Quenching at 1080°C and sensitization heating at 650°C for one hour increase the corrosion rate from 0.190 mm/year in steel containing 0.14% silicon to 0.489 mm/year in steel containing 0.78% silicon, i.e. by a factor of 2.5.

Table 3. Corrosion resistance of the sensitized (at 650°C, 1 h) stainless steels in a boiling 65% nitric acid solution

Concentration of an element			Average corrosion rate, mm/year
C, wt %	Si, wt %	other elements, wt %	
0.022	0.14	–	0.190
0.021	0.38	–	0.248
0.021	0.38	0.0015 B	**2.506**
0.021	0.38	0.042 REMs	0.234
0.020	0.78	–	0.489
0.030	0.78	–	**16.340**

Unsatisfactory IGC resistance is highlighted in bold.

Nevertheless, we cannot ignore the fact that even the corrosion loss at a high silicon content (0.78 wt %) and a low carbon content (0.020 wt %) does not exceed the critical limit. An increase in the carbon concentration by only 0.01 wt % (03Kh18N11GS0.78 steel) greatly increases the corrosion rate from 0.489 to 16.340 mm/year, i.e. more than 30 times.

The examination of the steel microstructure and grain boundary state in the samples tested by the DU technique after sensitization heating provided evidence of the negative influence of sensitization on the tendency of stainless steel to intergranular corrosion in boiling nitric acid. Increased and almost continuous etching of grain boundaries was observed in the steel with high silicon content and a lower etching, in the steel with low silicon content.

The TEM study of the foils showed that sensitization heating after quenching in the steel with low silicon concentration (0.14 wt %) does not cause noticeable changes in the state of grain boundaries (Fig. 1a), while in the steel with high silicon content (0.78 wt %) it results in the precipitation of chains or colonies of dispersed excess phase particles at grain boundaries (Fig. 1b).

The electron diffraction pattern taken from one of the precipitates indicated by the arrow in Fig. 1b shows that it is a single crystal and is coherently matched to the matrix. The calculation of the total diffraction pat-

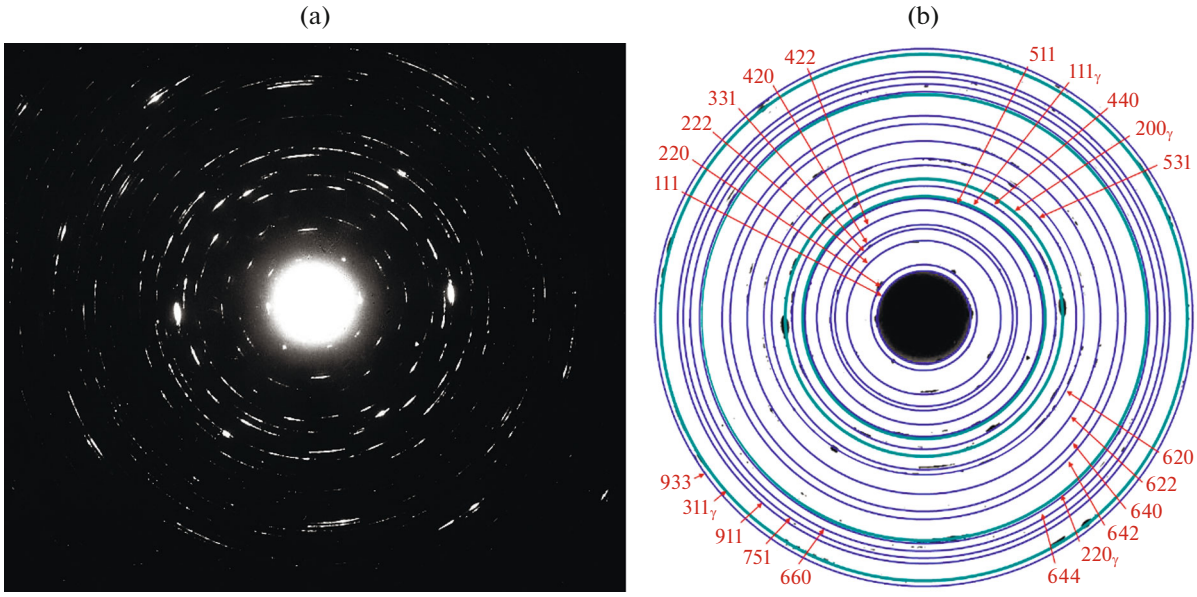

Fig. 2. Electron diffraction pattern of the quenched 02Kh18N11GS0.78 steel after (a) sensitization heating at 650°C for 10 h and (b) its indexing.

tern taken from the region of the 02Kh18N11GS0.78 steel foil (Fig. 2) shows that the unit cell of the excess phase is almost three times larger than that of the matrix and corresponds, like the austenitic matrix, to the FCC lattice. The calculation showed that silicon virtually did not change the size of the austenite unit cell at a distance from the grain boundary, where a = 3.565 Å, and significantly decreases the lattice parameter (a) to 3.530 Å in the boundary volumes. The lattice parameter of the identified investigated phase, which is a $Cr_{23}C_6$ compound, is 10.615 Å and differs slightly from the lattice parameter of carbide, which is 10.65 Å.

The results are in agreement with those of [13]. That work studied the effect of the silicon content (0.09–1.03 wt %) on the IGC resistance of the 12Kh18N10T steel in nitric and sulfuric acids. The study revealed a low IGC resistance of samples with high silicon content. The authors of that paper believe that the mechanism of the formation of such nonequilibrium silicon segregations is based on the (hypothesis of) impurity accumulation near boundaries due to the movement of "vacancy-impurity atomic complexes" to grain boundaries and fixation of this state during quenching. Moreover, the authors assume that the structure imperfection near grain boundaries can develop due to increasing dislocation density and vacancy accumulation.

The same was demonstrated in [14], where dislocations in the 03Kh18N11 (AISI 304L) steel with low silicon content (less than 0.1 wt %) arranged themselves as uniformly distributed cells throughout the body and at grain boundaries, whereas coplanar accumulations of dislocations along grain boundaries are observed in high-silicon steels with 0.8% Si, and their number is twice greater than in the grain volume.

The obtained results therefore allow us to conclude that $Cr_{23}C_6$ compounds with a changed lattice parameter (mismatch is ~0.33%) precipitate along grain boundaries in low-carbon Cr–Ni steels with a silicon concentration close to the upper limit (0.78 wt %) after quenching from 1080°C during subsequent heating at 650°C. They precipitate due to some amount of silicon, which has a smaller atomic radius than chromium (1.18 and 1.28 Å, respectively), incorporated into the carbide.

These inclusions have a certain orientational relationship with an adjacent matrix layer. A coherent matching between the excess phase and austenite becomes possible due to a decrease in the austenite lattice parameter from 3.565 to 3.530 Å (about 1%) near the carbide inclusions, with the carbide lattice parameter differing by a factor of three from the austenite lattice parameter. The decrease in the austenite lattice parameter in the narrow interphase zone indicates solid solution decomposition. Silicon, as a horophilic element, concentrates at grain boundaries and dissolves in the matrix according to the substitution principle. It reduces the lattice parameter of austenite, creating a solid matrix-silicon solution of a certain and constant composition. The width of the austenite layer with a smaller lattice parameter, i.e. the degree of austenite decomposition, a state determining the readiness for the excessive phase to precipitate along the grain boundaries, depends on the silicon content in the steel and the preheating treatment (heating temperature, holding time, and others).

Table 4. Corrosion resistance of quenched and sensitized (at 650°C, 1 h) stainless steels with different nitrogen and carbon concentrations in a boiling 65% nitric acid solution

Concentration of an element		Austenitizing temperature, °C	Average rate of corrosion, mm/year
C, wt %	N, wt %		
0.025	0.30	1050	0.252
		1100	0.217
0.030	0.27	1050	0.382
		1100	0.204
0.060	0.23	1050	**6.706**
		1100	**7.400**
0.052	0.21	1050	**7.202**
		1100	**6.357**
0.037	0.16	1050	**1.023**
		1100	**0.716**

Testing by DU technique in boiling 65% nitric acid solution has shown that steels with a high nitrogen concentration (0.16–0.30 wt %) and a low carbon concentration (less or equal to 0.03 wt %) possess high corrosion resistance (Table 4). The corrosion rate at an increased carbon content to 0.037, 0.052, and 0.060 wt % in the same alloying system increases to 6–7 mm/year (Table 4).

Electron microscopic studies show that a high corrosion resistance is characterized by lower dislocation density, which can be clearly seen at interphase zones and coherent twin boundaries (Fig. 3). The dislocations are distributed irregularly and form a cellular structure (Figs. 3a, 3b). However, a high dislocation density is observed in 06Kh20N9G3A0.23 steel with a high carbon concentration and a low corrosion resistance (Fig. 3c). A high dislocation density, stacking faults, and microstress fields around them are thermodynamically advantageous places for the location (segregation) of a large number of impurity atoms, particularly carbon (Cotrell atmosphere principle). This causes the formation of local electrochemical cells, the selective dissolution of active anode sites, and the facilitated formation of chromium carbides and chromium-depleted solid solution.

To find the temperature-time range where nitrided 03Kh20N9G3A0.30 steel exhibits a tendency to intergranular corrosion, we plotted a Rollason diagram after sensitization heating at various temperatures and after testing in a boiling 65% solution of nitric acid (Fig. 4). The diagram shows that after sensitization heating for 1 h at 650°C, the corrosion rate of the 03Kh20N9G3A0.30 steel is 0.22 mm/year. The depth of intergranular corrosion penetration in this case reaches 20 μm. A comparison of the 03Kh20N9G3A0.30 and 3Ch18Ni11 steels shows that the critical holding time of the nitrogen-containing steel increases to 16 hours at 650°C, and the range where this steel tends to inter-

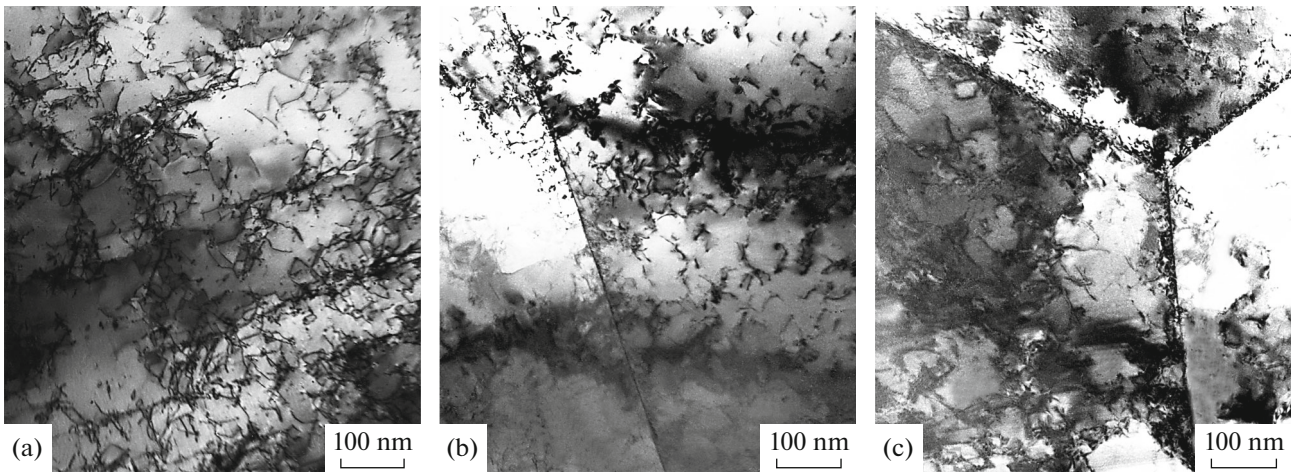

Fig. 3. Fine structure of the (a), (b) 03Kh20N9G3A0.30 steel with a high corrosion resistance and (c) 06Kh20N9G3A0.23 with a low corrosion resistance. Heat treatment regime for the samples: (a), (c) quenching from 1050°C, 30 min, water + heating at 650°C, 1 h, air, and (b) quenching from 1100°C, 30 min, water + heating at 650°C, 1 h, air.

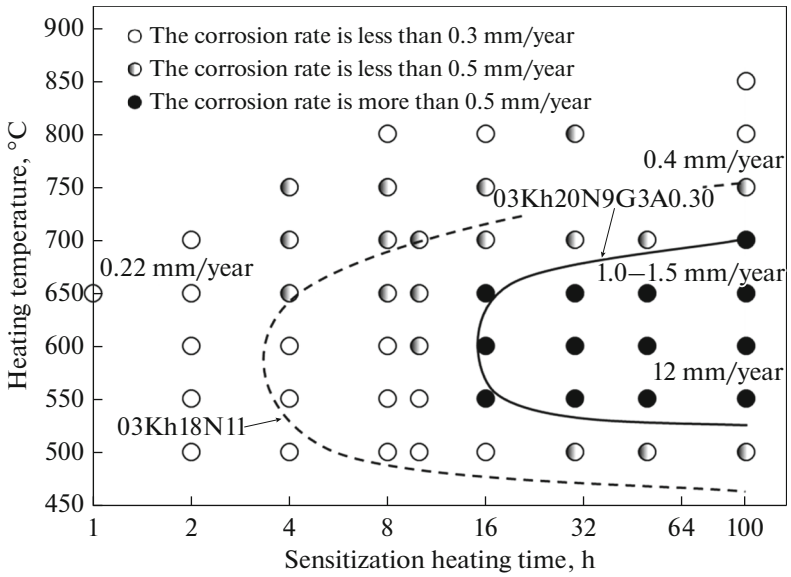

Fig. 4. Region where sensitized 03Kh18N11 (bounded by the dashed curve) and 03Kh20N9G3A0.30 (by the solid one) steels tend to intergranular corrosion in a boiling 65% nitric acid solution. The experimental data for 03Kh20N9G3A0.30 steel are indicated by dots: ○ the corrosion rate is less than 0.3 mm/year; ◐ the corrosion rate is less than 0.5 mm/year; ● the corrosion rate is more than 0.5 mm/year.

granular corrosion shifts to the right towards longer holding times. Heating at 600 and 650°C for 100 h causes sensitization and an increase in the corrosion rate to 1.0–1.5 mm/year. The steel structure exhibits excessive phases, such as chromium carbides and nitrides.

Hundred-hour heating at a lower temperature of 550°C results in the precipitation of much more carbides than nitrides, which increases the penetration depth of intergranular corrosion above 70 μm and increases the corrosion rate to 12 mm/year.

There is no way to distinguish the direct influence of carbides and nitrides on intergranular corrosion. However, the main role in the occurrence and development of IGC seems to belong to chromium carbides. This is proven by the fact that when nitrides precipitate above 750°C, the corrosion rate is very low (only 0.4 mm/year after 100 hours of exposure at 750°C). On the other hand, the corrosion rate is very high (12 mm/year) during a 100-h sensitization heating at 550°C, when mostly chromium carbides precipitate. This can be explained by the fact that $Cr_{23}C_6$ carbides stoichiometrically contain rather larger amounts of chromium than Cr_2N nitrides do. This increases the chromium depletion of the interphase regions and the development of intergranular corrosion.

Corrosion tests of sensitized nitrogen austenitic steels microalloyed with boron or rare-earth metals revealed that the introduction of these elements in small amounts (boron to 0.0024 wt %, REMs to 0.037 wt %) has no negative effect on IGC. Corrosion losses of the 03Kh20N9G3A0.30 steel alloyed with small additions of boron and REMs during testing by the DU technique do not exceed 0.35 mm/year (Table 5). However, the corrosion rate increases to 1.328 mm/year and grain boundaries are etched to a greater extent when the boron concentration is increased to 0.01 wt %. Microalloying of chromium-nickel austenitic steels with large amounts of REMs results in low etching of regions at grain boundaries. The excess phase is clearly identified at grain boundaries in the stainless steel alloyed with 0.01 wt % boron after sensitization heating (Fig. 5).

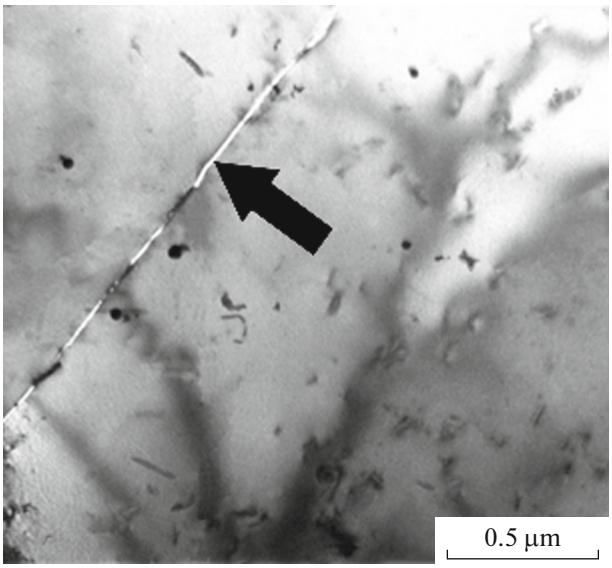

Fig. 5. Precipitates along grain boundaries in the steel containing 0.01 wt % boron after quenching from 1080°C and 10-h heating at 650°C.

Table 5. Effect of boron and REM microalloying on the corrosion resistance of 03Kh20N9G3A0.30 steel in a boiling 65% nitric acid solution

Steel	Concentration of an element			Average corrosion rate, mm/year
	C, wt %	N, wt %	Other elements, wt %	
03Kh20N9G3A0.30	0.025	0.30	–	0.252
03Kh20N9G3A0.29R	0.023	0.29	0.0015 B	0.275
			0.0024 B	0.332
			0.01 B	**1.328**
03Kh20N9G3A0.29Ch	0.025	0.29	0.02 REMs	0.189
			0.016 Y	0.220
			0.020 Y	0.230
			0.037 Y	0.220

The particles of this excess phase (indicated by an arrow in the electron diffraction patterns) are identified as $Cr_{23}(C,N,B)_6$ carboborides and Cr_3B_4 borides. The precipitation of the considerable amounts of $Cr_{23}(C,N,B)_6$ carboborides and Cr_3B_4 borides, which form an almost continuous interlayer between grains, depletes the boundary regions significantly of chromium. This increases the rate of intergranular corrosion when the concentration of boron is increased.

CONCLUSIONS

(1) A decrease in the silicon concentration from 0.78 to 0.14 wt % in the Cr–Ni austenitic steels increases the corrosion resistance of these steels in the quenched and, especially, the sensitized state. The precipitation of $Cr_{23}C_6$ carbides at the grain boundaries was shown to be responsible for the low corrosion resistance of the sensitized steel. Increasing the silicon concentration to 0.78 wt % intensifies this process, resulting in the separation of austenite into silicon-rich and silicon-depleted solid solution.

(2) The conditions under which the nitride Cr–Ni 03Kh20N9G3A0.30 steel is resistant to intergranular corrosion were found. The main role in the development of IGC was determined to be played by chromium carbides precipitated during sensitization. The chromium carbides deplete the boundary regions of chromium to a greater extent than nitrides.

(3) Microalloying of the nitrogen austenitic steel even with small amounts of boron (0.01 wt %) was revealed to deteriorate its resistance to intergranular corrosion upon provoking heating. This can be explained by the precipitation of a continuous layer of Cr_3B_4 borides and $Cr_{23}(C,N,B)_6$ carboborides along grain boundaries, thereby considerably depleting boundary regions of chrome and increasing the corrosion rate. On the contrary, microalloying of similar Cr–Ni steel with larger amounts of REMs (0.037 wt %) did not deteriorate its corrosion resistance.

(4) Electron microscopic studies showed that the high corrosion resistance can be achieved at low density of irregularly distributed dislocations forming a cellular microstructure. However, a high dislocation density makes the microstress fields around them thermodynamically favorable places for the segregation of a large number of impurity atoms. This results in the formation of local electrochemical cells with selective dissolution of the active anode sites, facilitates the formation of chromium carbides, and depletes the solid solution of chromium.

REFERENCES

1. V. V. Naumenko, Candidate's Dissertation in Engineering (Moscow, 2012).
2. R. Robin, F. Miserque, and V. Spagnol, "Correlation between composition of passive layer and corrosion behavior of high Si-containing austenitic stainless steels in nitric acid," J. Nucl. Mater. **375**, No. 1, 65–71 (2008).
3. B. E. Wilde, "Influence of silicon on the intergranular corrosion behavior of 18Cr–8Ni stainless steels," Corros. Sci. **44**, No. 10, 699–704 (1988).
4. O. V. Kasparova, "Peculiarities of intergranular corrosion of silicon-containing austenitic stainless steels," Prot. Met. **40**, No. 5, 475–481 (2004).
5. S. Ningshen, U. K. Mudali, G. Amarendra, and B. Raj, "Corrosion assessment of nitric acid grade austenitic stainless steels," Corros. Sci. **51**, No. 2, 322–329 (2009).
6. K. Huang and R. E. Logé, "Microstructure and flow stress evolution during hot deformation of 304L austenitic stainless steel in variable thermomechanical conditions," Mater. Sci. Eng. **711**, 600–610 (2018).
7. M. V. Pridantsev, *Influence of Impurities and Rare Earth Elements on the Properties of Alloys* (Metallurgizdat, Moscow, 1962) [in Russian].

8. K. A. Lanskaya, *Heat Resistant Steels* (Metallurgiya, Moscow, 1969) [in Russian].
9. Yu. N. Goykhenberg, L. G. Zhuravlev, D. A. Mirzayev, V. V. Zhuravleva, Ye. P. Silina, and V. Yu. Vnukov, "Corrosion cracking, structure and properties of hardened Cr–Mn austenitic steels with nitrogen," Phys. Met. Metallogr. **65**, No. 6, 83–89 (1988).
10. L. G. Korshunov, Yu. N. Goikhenberg, and N. L. Chernenko, "Influence of silicon on the structure, tribological and mechanical properties of nitrogen-containing Cr–Mn austenitic steels," Fiz. Met. Metalloved. **96**, No. 3, 100–110 (2003).
11. S. Yu. Mushnikova, S. K. Kostin, V. V. Sagaradze, and N. V. Kataeva, "Structure, properties, and resistance to stress-corrosion cracking of a nitrogen-containing austenitic steel strengthened by thermomechanical treatment," Phys. Met. Metallogr. **118**, No. 11, 1155–1166 (2017).
12. V. V. Sagaradze, N. V. Kataeva, I. G. Kabanova, S. V. Afanas'ev, and A. V. Pavlenko, "Effect of the temperature of shock-wave loading on structure and phase transformations in nitrogen-containing austenitic Cr–Mn–Ni steel, Phys. Met. Metallogr. **121**, No. 7, 683–688 (2020).
13. Yu. P. Solntsev, B. S. Ermakov, and S. O. Malikov, "Role of Si in the formation of the corrosion resistance of austenitic materials for cryogenic engineering," Russ. Metall. (Metally). **2**, 133–137 (2008).
14. B. S. Ermakov and Yu. P. Solntsev, "Intergranular corrosion as a major factor in increased destruction of equipment made from austenitic steels," Baltiiskie Metally, No. 2, 18–21 (2000).

Translated by T. Gapontseva